Is it possible the *ab initio* thermodynamics with defects?

In Gee Kim
Computational Metallurgy Laboratory,
GIFT, POSTECH, Pohang 790-784

Phase-Diagrams: The first-step of materials design

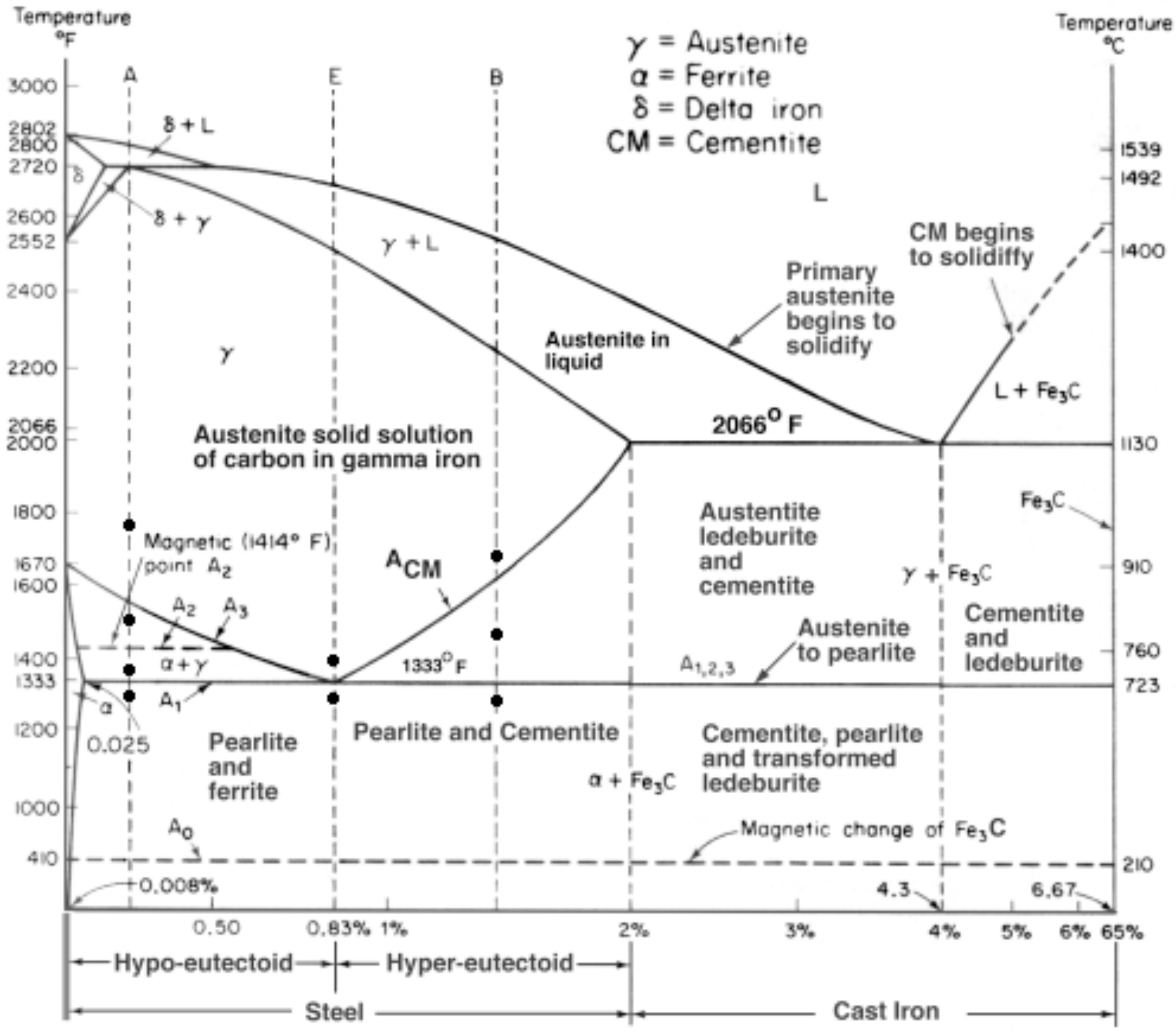

Fe-Fe_3C Phase Diagram, *Materials Science and Metallurgy*, 4th ed., (Pollack, Prentice-Hall, 1988)

Process design with kinetics

Russel, *Acta Metal.* **17**, 1123 (1969)

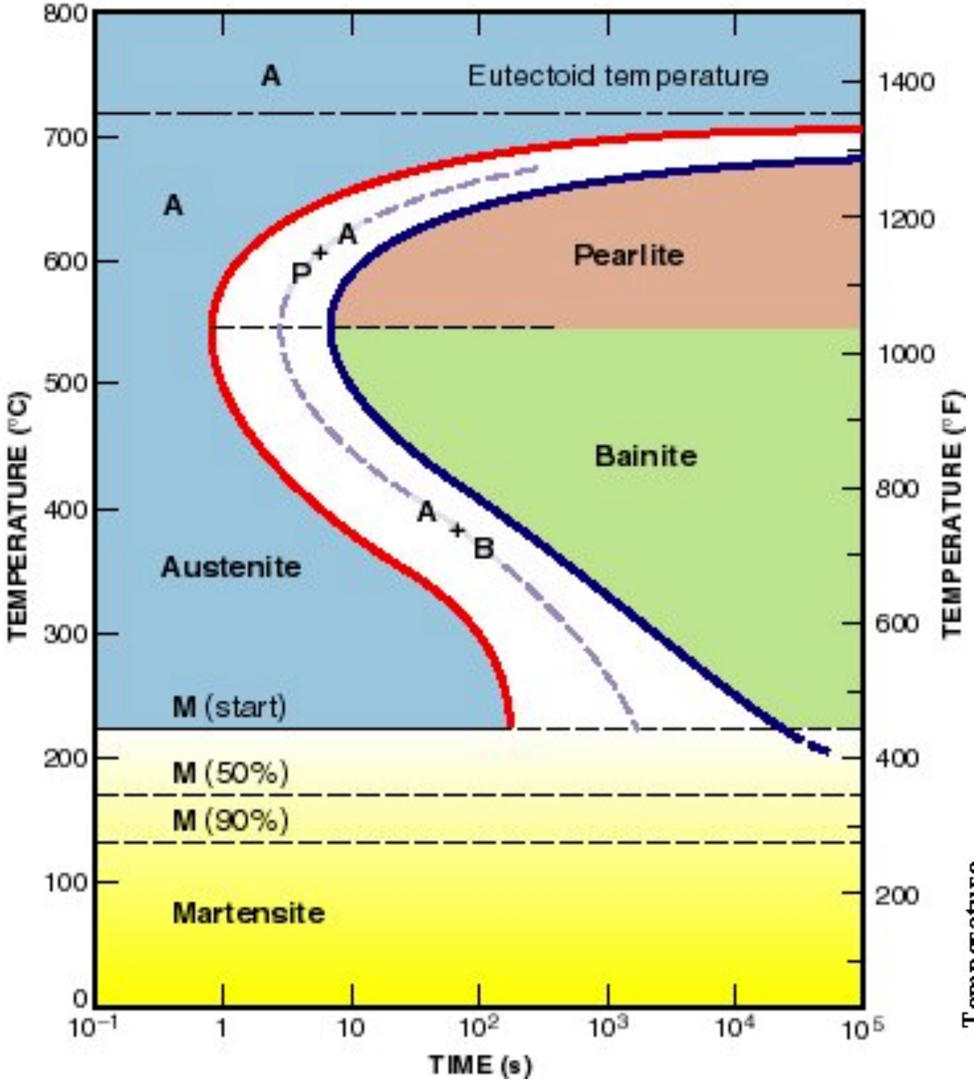

TTT Diagram

Bhadeshia, *Metal. Sci.* **16**, 159 (1982)

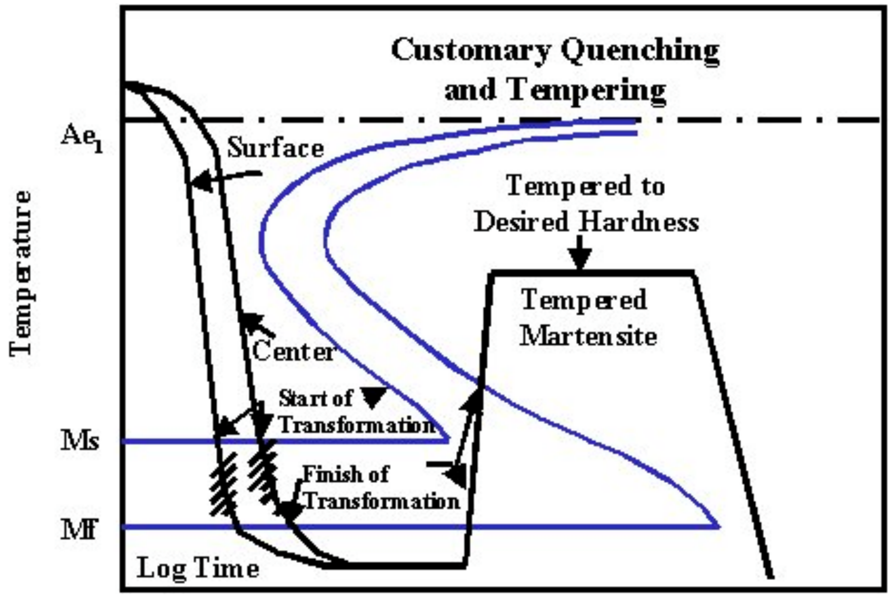

Defects generate heat, e.g., Potevine-LeChatelier (PLC) effect

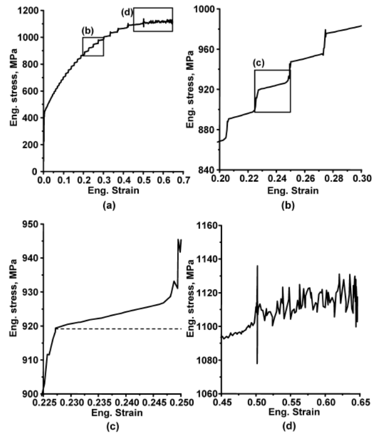

Fig. 1. (a) Stress–strain curve of Fe0.6C18Mn TWIP steel. (b) Enlargement of the first boxed segment of the stress–strain curve exhibiting type A serrations, characterized by a steep rise in stress alternating with plateau-like features. (c) Enlargement of a typical type A serration. The steep rise corresponds to the initiation of a PLC band outside the strain gauge measuring range. The plateau segment corresponds to the passage of the PLC band in the strain gauge measuring range. The increase in stress in the plateau segment, suggests strain hardening in the region outside the PLC band. (d) Enlargement of the type B serrations, characterized by a unstable serration pattern.

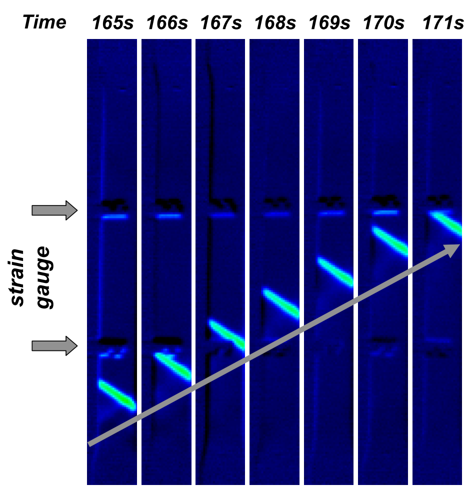

Chen *et al.*, *ISIJ Int.* **47**, 1804 (2007)

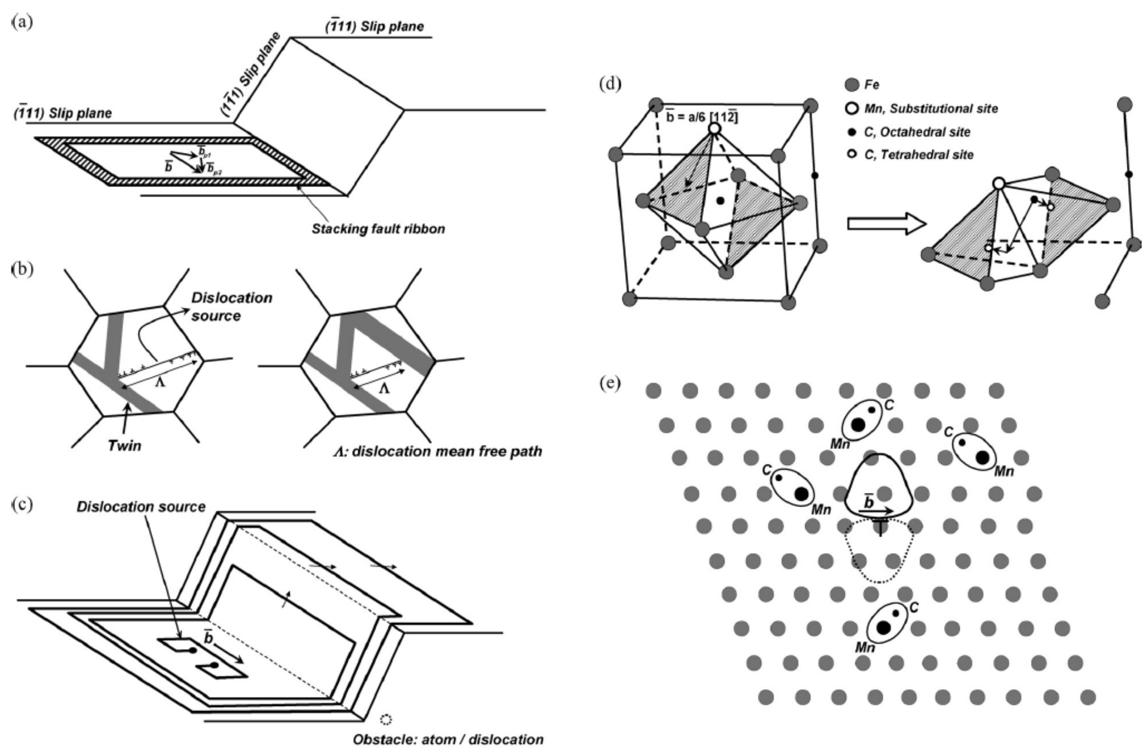

Fig. 8. (a) Low SFE model: a low SFE leads to widely dissociated partial dislocations, which cannot cross slip. This pronounced planar slip results in a high strain hardening rate. (b) Dynamic Hall–Petch model of Bouaziz–Guelton: at low SFE, twinning is promoted. The intersection of twins forms a cell structure. The twin boundaries act as obstacle for dislocation glide. (c) Planar slip model: in concentrated solid solution alloys short range order (SRO) is possible and dislocations will destroy the SRO on their slip plane. Whereas the leading dislocation experiences a high resistance to its motion, subsequent dislocations can glide more easily in the same slip plane. This favors planar slip and result in a high rate of strain hardening. (d) Illustration of the reduction of the SRO during the passage of partial dislocation on their glide plane: the octahedral clusters are sheared and the C atoms are transferred to tetrahedral interstitial sites. Left: before slip. Right: after slip. (e) Dastur–Leslie model: dynamic stain aging in FeMnC alloy is caused by the re-orientation of Mn–C cluster in the dislocation stress field during dislocation motion.

A material as a system by multiscale simulation

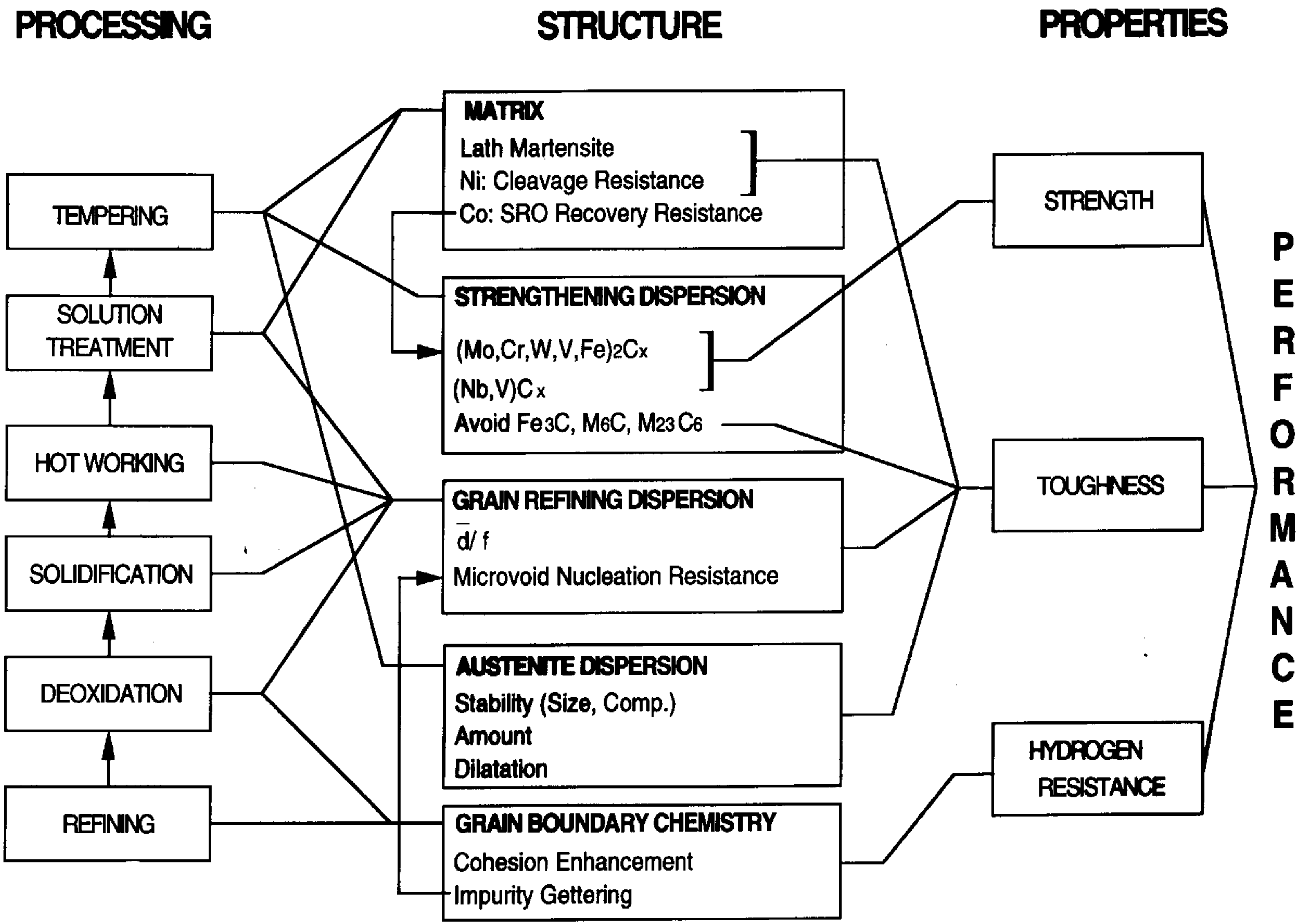

Courtesy by G. B. Olson, Dept. MSE, Northwestern Univ., USA

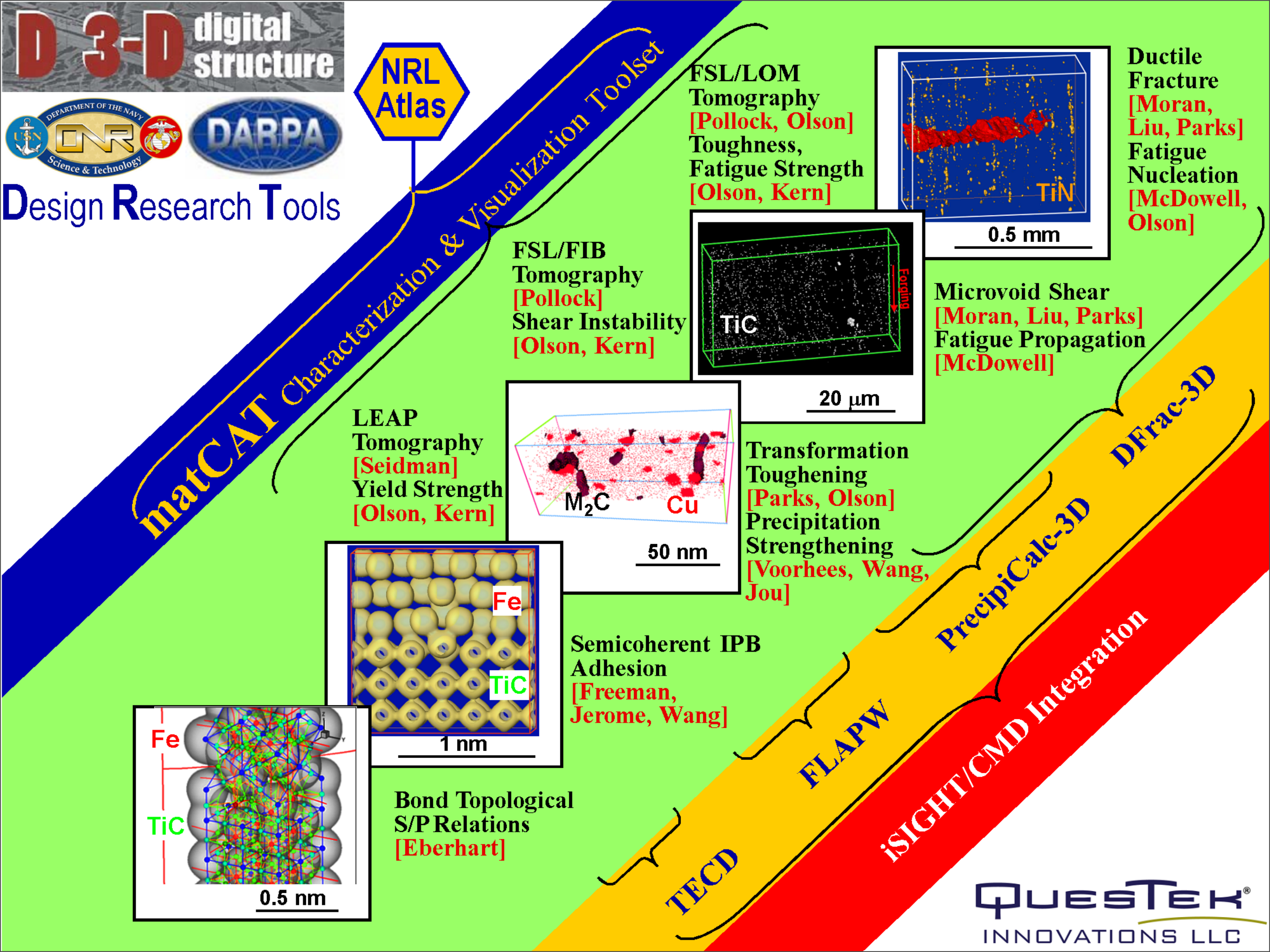
D 3-D digital structure
DEPARTMENT OF THE NAVY
ONR
Science & Technology
DARPA
Design Research Tools
NRL Atlas
matCAT Characterization & Visualization Toolset
FSL/LOM
Tomography
[Pollock, Olson]
Toughness,
Fatigue Strength
[Olson, Kern]
TiN
0.5 mm
Ductile
Fracture
[Moran,
Liu, Parks]
Fatigue
Nucleation
[McDowell,
Olson]
FSL/FIB
Tomography
[Pollock]
Shear Instability
[Olson, Kern]
TiC
Forging
20 μm
Microvoid Shear
[Moran, Liu, Parks]
Fatigue Propagation
[McDowell]
LEAP
Tomography
[Seidman]
Yield Strength
[Olson, Kern]
M2C
Cu
50 nm
Transformation
Toughening
[Parks, Olson]
Precipitation
Strengthening
[Voorhees, Wang,
Jou]
Fe
TiC
1 nm
Semicoherent IPB
Adhesion
[Freeman,
Jerome, Wang]
Fe
TiC
0.5 nm
Bond Topological
S/P Relations
[Eberhart]
DFrac-3D
PrecipiCalc-3D
FLAPW
TECD
iSIGHT/CMD Integration
QuesTek
INNOVATIONS LLC

Technology Transfer

QuesTek® Navy Alloy Designs

Marine Corps: M67854-05-C-0025

NAVAIR: N68335-05-C-0207 and N68335-07-C-0108

ONR: N00014-05-M-0250
NAVAIR: N68335-06-C-0339

ONR: N00014-07-M-0445 STTR-I

NAVAIR: N68335-07-C-0428

NAVAIR: N68335-07-C-0302 and N68335-08-C-0288

Navy/ONR: N00014-05-C-0241

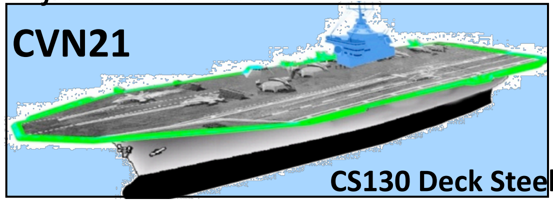

Navy: In-contracting

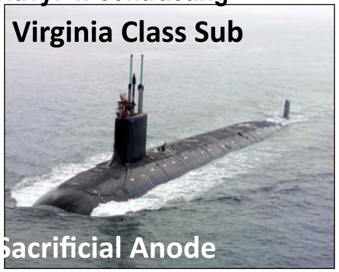

ONR: N00014-09-M-0220

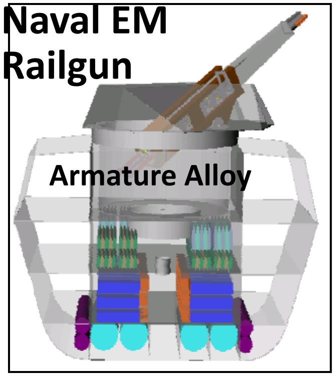

NAVAIR: N68335-09-C-0215

ONR: N00014-08-M-0309

Topological defects ➔ The prophecy of P. W. Anderson

P. W. Anderson

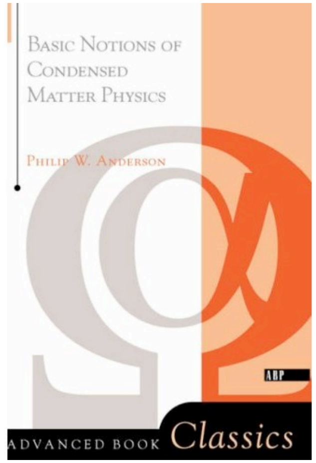

“I do **not** accept that this is a philosophical difficulty,
or that it demonstrates anything like an impossibility *in principle*
of **treating macroscopic objects quantum-mechanically**;
merely that this discussion brings out the *practical* problems of
determining all the relevant phases in a given system.”
In *Basic Notions of Condensed Matter Physics* (Addison Wesley, 1997) p. 51.

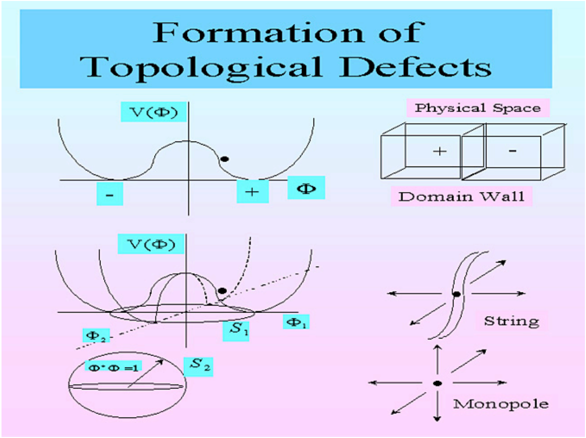

http://aether.lbl.gov/eunhwa_webpage_2/whynot.html

Boyer and Viñals, *Phys. Rev. E* **65**, 046119 (2002)

$$\frac{\partial\psi}{\partial t}=\epsilon\psi-\frac{1}{k_0^4}(k_0^2+\nabla^2)^2\psi-\psi^3,$$

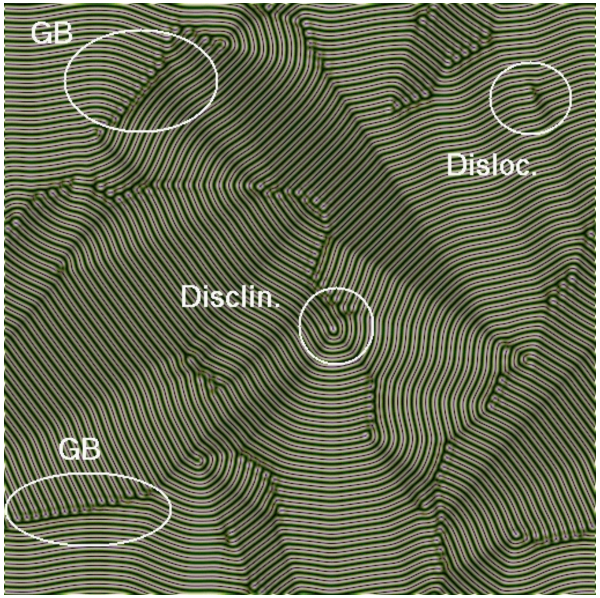

Zurek-Kibble domain structure: *Phys. Rev. Focus,* 12 May 2006

$$\frac{\partial^2\zeta}{\partial t^2}+\frac{2}{t_d}\frac{\partial\zeta}{\partial t}-\Delta\zeta-\frac{2}{R^2}\zeta=0,$$

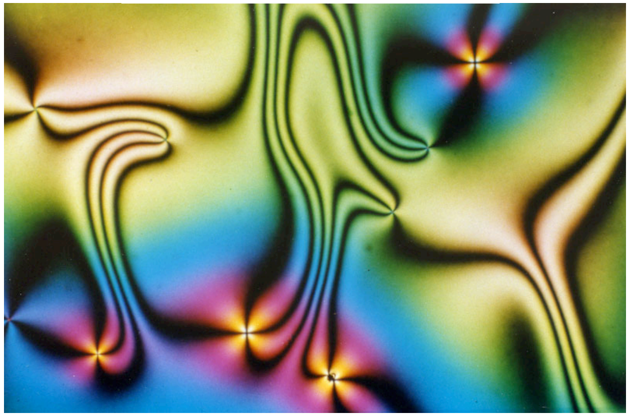

Geometric theory of defects

Katanaev, *Phys. Usp.* **48**, 675 (2005)

Elastic deformation (Euclidean)

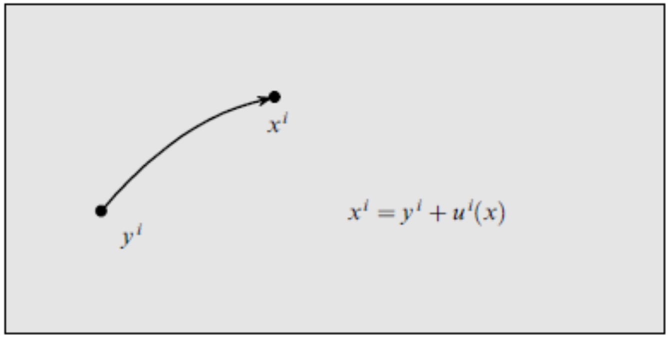

The ground undeformed state of the medium
➔The external observer fixes
a Cartesian coordinate system (Gauge fixing).
The deformed medium,
➔ The external observer discovers
that the metric becomes nontrivial
in this coordinate system.

Riemann-Cartan manifold theory

Levi-Civita connection (Christoffel symbols)

torsion

nonmetricity

Curvature tensor of the affine connection

Topological defects

➔

Einstein equation for 3D gravity

Example: Dislocations

Burgers vectors constructed by the Volterra process

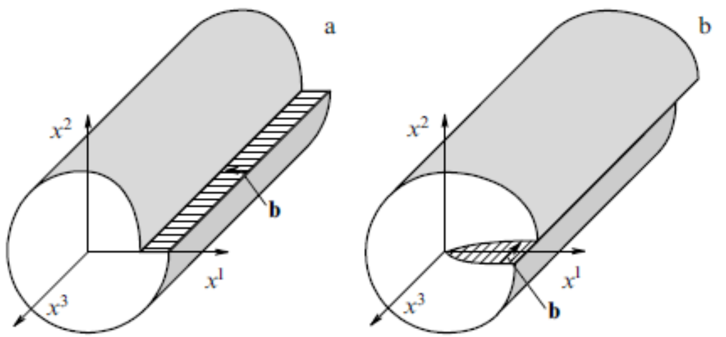

Figure 2. Straight linear dislocations. (a) The edge dislocation. The Burgers vector **b** is perpendicular to the dislocation line. (b) The screw dislocation. The Burgers vector **b** is parallel to the dislocation line.

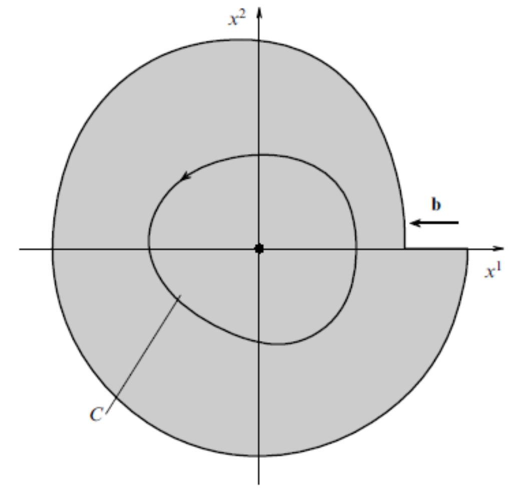

Figure 3. Section of the medium with the edge dislocation. C is the integration contour for the Burgers vector **b**.

Introduce a vielbein

- Invariant under arbitrary coordinate transformation,
- Covariant under global SO(3) rotations of y^i.

With the Cartan torsion tensor T

Single-particle quantum motion on a Riemann-Cartan manifold

Bausch *et al.*, *Phys. Rev. Lett.* **80**, 2257 (1998)

The tight-binding Hamiltonian

The distortions by defects

The affine connection and the covariant derivative

with the torsion tensor, measures the defect density.

The new Hamiltonian with defects for the continuum limit $a \rightarrow 0$

Aharonov-Bohm effect of the spin wave by a screw dislocation

Turski and Mińkowski, *J. Phys. C: Condens. Matter* **21**, 376001 (2009)

We shall now present the solution of equation (10) for a single screw dislocation along the z axis with the Burgers vector $\boldsymbol{b} = b\boldsymbol{e}_z$. The only nonvanishing components of the Kröner distortions β^i_j are then $\beta^3_i, i = 1, 2$:

$$\begin{aligned} \beta^3_1 &= -\frac{b}{2\pi}\partial_2 \ln\sqrt{(x^1)^2 + (x^2)^2} \\ \beta^3_2 &= \frac{b}{2\pi}\partial_1 \ln\sqrt{(x^1)^2 + (x^2)^2}. \end{aligned} \tag{11}$$

Assuming in the cylindrical coordinates $\Psi(r, \phi, z, t) = \chi(r, \phi)\exp(\mathrm{i}kz + \mathrm{i}\omega t)$ we found that the envelope $\chi(r, \phi)$ obeys the Aharonov–Bohm equation [18]:

$$\left[\frac{\partial^2}{\partial r^2} + \frac{1}{r}\frac{\partial}{\partial r} + \frac{1}{r^2}\left(\frac{\partial}{\partial \phi} + \imath\alpha\right)^2 - q^2\right]\chi(r, \phi) = 0, \tag{12}$$

where $\alpha = kb/2\pi$ and $q^2 = k^2 + 2\mu\omega$. Using the asymptotic $r \to \infty$ solution for that equation [12, 18–20] and recalling the definition of the function Ψ we found

$$\begin{aligned} \begin{pmatrix} \delta S_x \\ \delta S_y \end{pmatrix} &= S_0 \begin{pmatrix} \cos \\ -\sin \end{pmatrix} (\alpha\phi + qr\cos\phi) \\ &+ \frac{\sin(\pi\alpha)}{\cos(\phi/2)\sqrt{2\pi qr}} \\ &\times \begin{pmatrix} \cos \\ \sin \end{pmatrix} (qr + \alpha(\phi - \pi)/2|\alpha| - \pi/4). \end{aligned} \tag{13}$$

In the absence of the dislocation the (pseudo)flux $\alpha = 0$ and we recover the standard spin wave solution of equation (1). The first term on the rhs of equation (13) shows the helical structure of the incoming spin wave due to global distortion of the lattice and the second describes the scattering phase shift due to the presence of dislocation. In figure 1 we have shown a Mathematica 7 generated density plot for the δS_y component of the solution (13). The δS_x component exhibits an identical structure with a trivial phase shift found from (13).

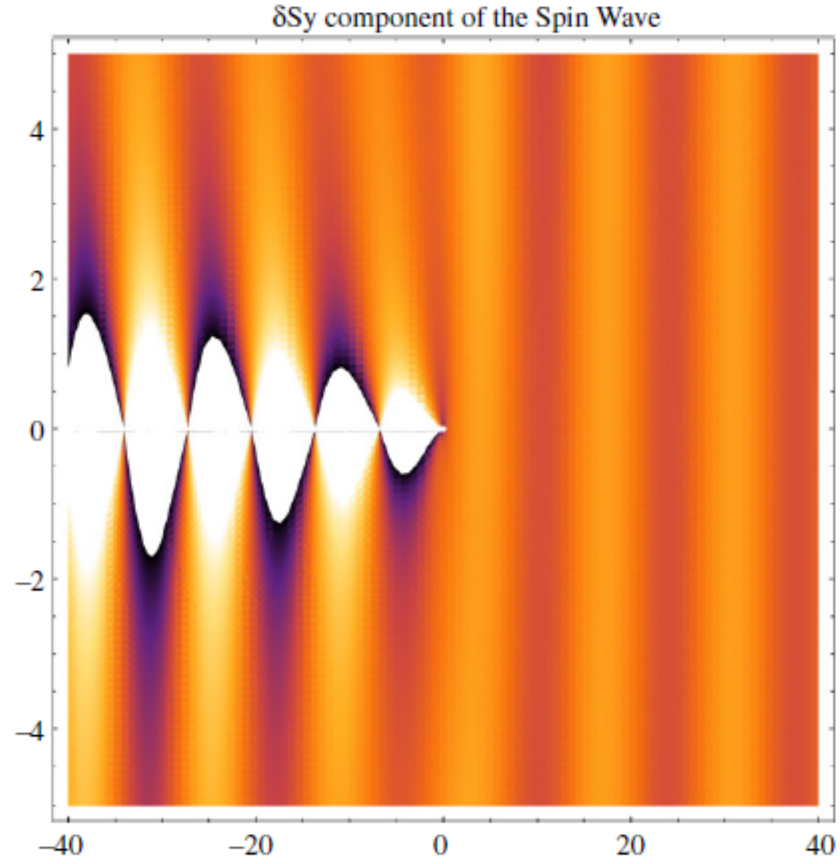

Figure 1. Mathematica 7 density plot for spin wave S_y solution equation (13). The wave is approaching from the right and deflects from the screw dislocation line located at the origin and perpendicular to the plot surface. The wavy edges of the cut to the left from the dislocations show the Aharonov–Bohm-like oscillations determined by the (pseudo)flux $\alpha = 0.4$.

Gauge theory of moving dislocations

Lazar, *Phys. Lett. A* **374**, 3092 (2010)

The dislocation density tensor and the dislocation current tensor

Satisfy the translational Bianchi identities,

The Lagrangian density

The equations of motion

By adding null Lagrangian, satisfying

momentum balance of dislocations

stress balance of dislocations

force balance of elasticity

Usual solution: massive fields Klein-Gordon equation

With (1+2)-dimensional d'Alembert operator,

Thermodynamics on flat space

Matsubara-Green-Kubo formalism

Grand canonical partition function, with

Statistical density matrix, follows the **Bloch equation**

By introducing the imaginary-time, the temperature Green's function

satisfies the Schwinger-Dyson equation as

with the noninteracting Green's function

In terms of the spectral function, the Lehmann representation of the Green's function is

$\rightarrow$

The corresponding real time Green's function is

Thermodynamics of black holes

Hartle-Hawking-Gibbons-Perry formalism

An action functional

The amplitude

The propagator

Introducing the negative imaginary parametric time

then

satisfies where

➔

S: the square of the Minkowski interval

For the metric,

with the Klein-Gordon Lagrangian density

the diffusion equation,

of the normal mode ψ yields the partition function

for small β.

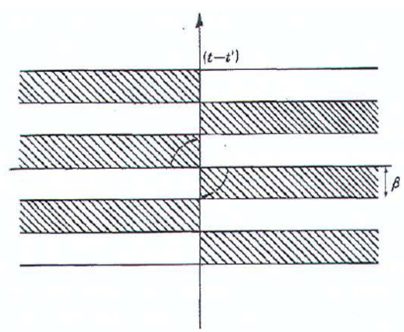

FIGURE 3. The complex $t-t'$ plane. G_T is analytic in the shaded regions. G_{E_T} is obtained by analytically continuing along the dotted paths. It is a periodic function of period $\beta = 1/T$.

Gibbons and Perry, *Proc. R. Soc. Lond. A* **358**, 467 (1978)

Hartle and Hawking, *Phys. Rev. D* **13**, 2188 (1976)

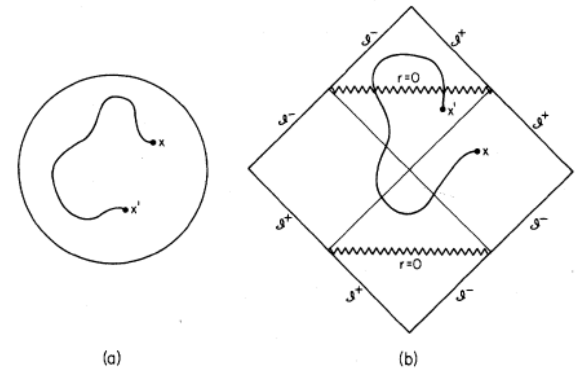

FIG. 2. (a) A compactified representation of a constant θ, constant φ slice of the positive-definite spacetime whose metric is given in Eq. (2.6). The heavy circle represents infinity. There are no singularities. A typical path connecting two points x' and x is shown. (b) A Penrose diagram for the Schwarzschild geometry showing in addition the regions of negative mass (or $r \leq 0$) above and below the singularities. A typical member of the class of paths continued analytically to this real section from the positive-definite spacetime represented in (a) is shown. Such paths may cross and recross the singularities at $r=0$. Integrations over paths which cross the singularities are specified by choosing contours of integration which are the analytic continuations of those in the positive-definite section.

Conclusion

- A fully quantum field theoretic formalism is available for thermodynamics with defects.
- This approach promises the authentic *ab initio* thermodynamics by eliminating *ad hoc* ones.
- Computational Practicality? See, below simulations by serious scientists.

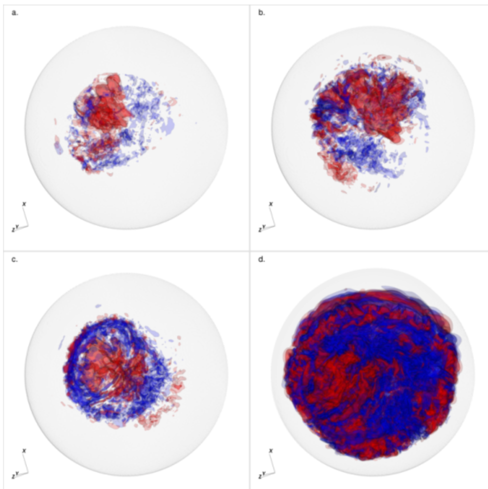

The radial velocity of the convection of a full white dwarf.
Appeared in *Astrophysical Journal* **704**, 196 (2009).

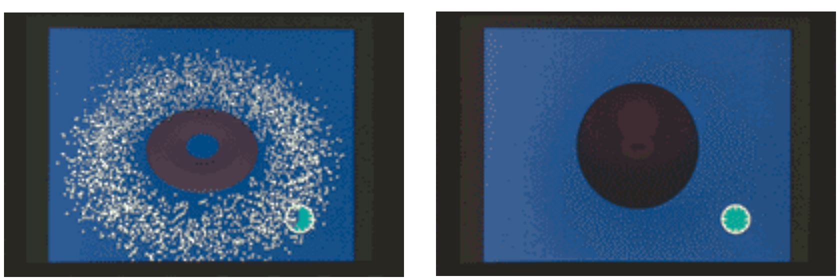

Matter collapse into a donut black hole.
Appeared in *Science* **275**, 476 (1997).

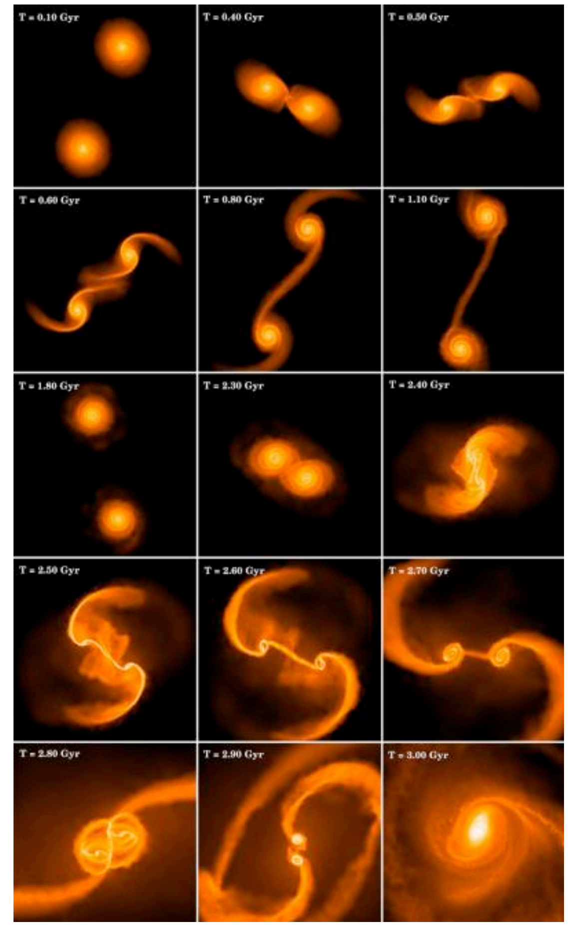

Two colliding galaxies.
By S. Kazantzidis, University of Chicago